



## Facile Synthesis, Characterization and *in vitro* Biological Evaluation of a Series of Sulfonylurea-linked Quinoline Derivatives as Potential Antimalarial Agents

SHARAN JEET KAUR KARAM SINGH<sup>1</sup>, KHAW LOKE TIM<sup>2</sup> and VASUDEVA RAO AVUPATI<sup>3,4,\*</sup>

<sup>1</sup>School of Postgraduate Studies, IMU University (Formerly known as International Medical University), 126, Jalan Jalil Perkasa 19, Bukit Jalil, 57000 Kuala Lumpur, Malaysia

<sup>2</sup>Department of Pathology and Pharmacology, School of Medicine, IMU University (Formerly known as International Medical University), 126, Jalan Jalil Perkasa 19, Bukit Jalil, 57000 Kuala Lumpur, Malaysia

<sup>3</sup>Department of Pharmaceutical Chemistry, School of Pharmacy, IMU University (Formerly known as International Medical University), 126, Jalan Jalil Perkasa 19, Bukit Jalil, 57000 Kuala Lumpur, Malaysia

<sup>4</sup>Centre of Excellence for Bioactive Molecules & Drug Delivery (BMDD), Institute for Research, Development & Innovation (IRDI), IMU University (Formerly known as International Medical University), 126, Jalan Jalil Perkasa 19, Bukit Jalil, 57000 Kuala Lumpur, Malaysia

\*Corresponding author: E-mail: [vasudevaraoavupati@gmail.com](mailto:vasudevaraoavupati@gmail.com)

Received: 21 January 2025;

Accepted: 25 March 2025;

Published online: 30 April 2025;

AJC-21973

World Health Organization (WHO) statistics showed that malaria has still remained a global threat due to its steady increase in deaths across the globe. Due to the necessity for novel pharmaceuticals, researchers discovered that a hybrid pharmacophore-designed methodology would be an effective means to develop new synthetic compounds and evaluate their efficacy against malaria. Therefore, a series of sulfonylurea-linked quinolines (**C1-C6**) were synthesized and evaluated for their *in vitro* antimalarial properties against *Plasmodium falciparum*. All the compounds (**C1-C6**) were screened through *in vitro* bioassays to assess their antimalarial potential against *P. falciparum* strain to identify the bioactive hit molecule; compounds were relatively compared with the clinically proven antimalarial agent *e.g.* artesunate. Based on the results, structure-activity relationships (SARs) have been derived that can be applied to design more analogues. Among the compounds tested, **C3** and **C2** were reported to be the most potent compounds with 68.10% and 65.55% inhibition of parasitemia in infected red blood cells (iRBC) compared to the positive standard artesunate with 64.98%, respectively. The *in vitro* antimalarial properties of compounds **C3** and **C2** were assumed to be primarily due to the presence of complementary pharmacophoric features such as sulfonylurea and quinoline, which formed part of the basic scaffold that was earlier independently well established as antimalarial pharmacophores.

**Keywords:** Facile synthesis, Sulfonylurea-linked quinolines, Structure-activity relationship (SAR), *in vitro* antimalarial properties.

### INTRODUCTION

In 2024, the world malaria report was published by the World Health Organization (WHO) that provides a clear statistic in malaria elimination and control globally. The estimated number of 263 million cases was reported across various regions globally in 2023, which is an increase of 11 million cases in comparison with the year 2022 [1]. Since the number of malaria cases is steadily increasing, there is an urgent need to discover novel bioactive antimalarial compounds to develop as drugs to treat malaria [2]. One of the key drivers of this increase is due to malaria drug resistance. The most common malaria causing helminth parasites are *Plasmodium falciparum*, *P. vivax*, *P. ovale*, *P. malariae* and *P. knowlesi*.

The transmission is mainly through a female Anopheles mosquito bite, which is the carrier of malaria-infected blood from one patient to the other, the main causative agent. Currently, as per WHO guidelines in the malaria treatment, artemisinin analogues (dihydroartemisinin, artemether, artesunate and artether) in combination with other antimalarial agents such as lumefantrine, amodiaquine, mefloquine, sulfadoxine and pyrimethamine are used as artemisinin-based combination therapies (ACTs) [3]. These combination therapies were proven to be effective in the process of eliminating infected parasites from the human body. However, there were several cases reporting on the development of resistance against artemisinin combinations as well [4]. Therefore, in this study, we designed

a series of novel sulfonylurea-linked quinoline analogues as potential antimalarial agents. The approach for the design of novel molecules is based on bioactive pharmacophore hybridization. Quinoline is the first ancient pharmacophore derived from the natural products that established several biological activities; among them, antimalarial potency is ancient [5]. Likewise, sulfonylurea derivatives have also been proven to be the most potent antimalarials based on experimental studies [6]. In alignment with our focused research interest in the synthesis of sulfonylurea derivatives as bioactive agents [7-11], using an evidence-based experimental design, we hybrid the sulfonylurea moiety into the quinoline antimalarial pharmacophore to synthesize, characterize and conduct *in vitro* antimalarial bioassay screening of hybrid sulfonylurea-quinoline analogues. The novelty of this study resides in, to the best of our literature search, there were no reports published highlighting the antimalarial properties specific to the compounds (C1-C6) or protocols reported in this study.

## EXPERIMENTAL

The reaction progress and the purity of the synthesized compounds were checked on pre-coated 60 F<sub>254</sub> silica gel TLC plates (USA, Merck, 0.25 mm) thickness by means of a gradient solvent system with *n*-hexane and ethyl acetate. Fourier-transform infrared (FT-IR) spectrometer (Japan, Shimadzu, Model: MIRAffinity-1S) was used to record the spectra. <sup>1</sup>H NMR & <sup>13</sup>C NMR spectra recorded on a Varian NMR System (USA, Varian, 500 MHz) using TMS (tetramethylsilane) as an internal standard. The electrospray ionization mass spectra (ESI-MS) were recorded using high-resolution mass spectrometry (HRMS) (USA, Thermo-Scientific, Q Exactive Focus, Orbitrap LC-MS/MS System). Melting point apparatus (U.K., Stuart Scientific, Model: SMP1) were determined in open capillary tubes and were uncorrected.

All the reagents and chemical were purchased from Sigma-Aldrich, USA, these includes *p*-toluenesulfonyl isocyanate, 4-amino-2-methyl-8-trifluoromethylquinoline, 4-amino-2-methyl-7-trifluoromethylquinoline 4-amino-6-fluoro-2-methylquinoline, 4-amino-7-trifluoromethylquinoline, 4-amino-7-fluoroquinoline, 4-amino-2,8-bis(trifluoromethyl)quinoline, anhydrous sodium sulphate, ethanol, chloroform and LC grade methanol, respectively. An incomplete malaria medium was prepared by dissolving 1 g glucose, 1.35 g sodium bicarbonate, 3 g of 4-(2-hydroxyethyl)-1-piperazineethanesulfonic acid (HEPES) in Hyclone RPMI 1640 (Thermo-Fisher Scientific, USA) which was then supplemented with Albumax II (0.5%, w/v), 30 µg/mL gentamicin and 50 µg/mL hypoxanthine (Merck, USA).

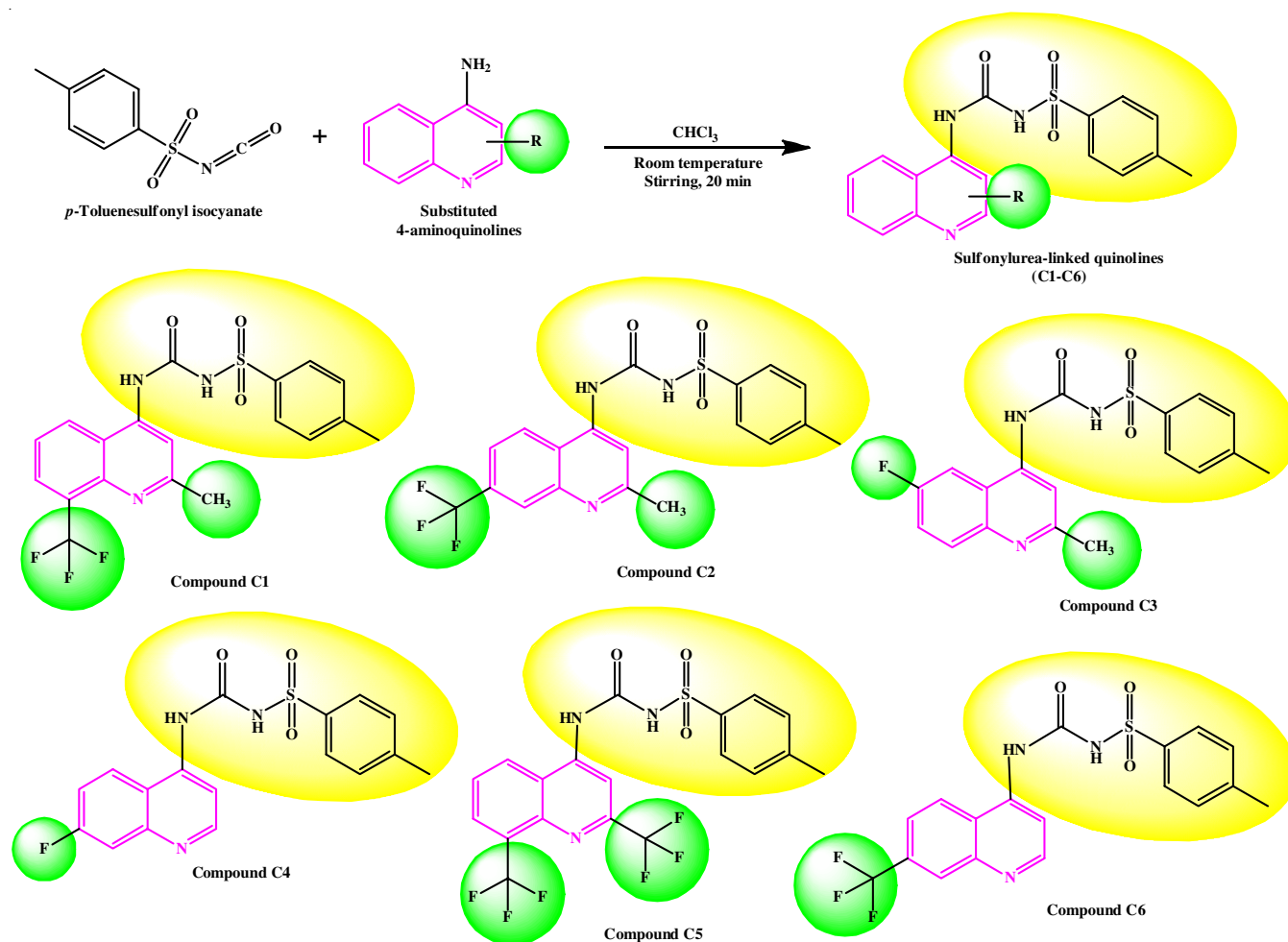
**General procedure for the synthesis of sulfonylurea-linked quinoline derivatives (C1-C6):** The facile synthesis method used in this study towards the synthesis of sulfonylurea-linked quinoline derivatives (C1-C6) is based on the standard reaction between *p*-toluenesulfonyl isocyanate with an amino quinoline reactant to produce resultant sulfonylurea-quinoline hybrids (C1-C6). The mole (0.01) concentration of 1:1 of the reactant A (*p*-toluenesulfonyl isocyanate) and reactant B (substituted aminoquinoline) was carefully measured and kept aside

for the reaction; initially, the pre-weighed reactant B was slowly added in portions to the quantity sufficient volume of chloroform (3-5 mL). The reaction mixture was made clear since gradually the solute slowly went into the chloroform. upon complete addition of reactant B, glass rod was used gently to stir at room temperature to make the reaction mixture homogeneous. Subsequently, once the reaction mixture was ready, reactant A charged into the syringe through the needle, without any delay, the reactant A was added to the reaction mixture quickly to prevent the oxidation of *p*-toluenesulfonyl isocyanate. Upon addition, the reaction mixture stirred using the glass rod for 20 min continuously until a solid amorphous powder precipitated. In the next step, the crude solid product formed in all experiments was subjected for the solvent washing chloroform to remove any traces of unreacted residues of reactant B, further the solids of crude products C1-C6 were treated with acetone and performed recrystallization (Scheme-I). The products obtained after recrystallization was filtered under vacuum filtration and dried in a hot air oven at controlled temperature of 45 °C, the dried solid was further used for the TLC analysis, melting point determination and spectral characterization.

**4-Methyl-N-((2-methyl-8-(trifluoromethyl)quinolin-4-yl)carbamoyl)benzenesulfonamide (C1):** Yield: 36%; yellow crystalline; m.p.: 122 °C; m.f.: C<sub>19</sub>H<sub>16</sub>F<sub>3</sub>N<sub>3</sub>O<sub>3</sub>S; relative molecular mass: 423; FT-IR (ATR,  $\nu_{\max}$  cm<sup>-1</sup>): 3349.45 (2° amide N-H *str.*), 3258.79 (2° amide N-H *str.*), 1688.71 (C=O *str.*), 1576.83 (aromatic C=C *str.*); <sup>1</sup>H NMR (500 MHz, DMSO-*d*<sub>6</sub>)  $\delta$  ppm: 2.35 (s, 3H, Ar-CH<sub>3</sub>), 2.56 (s, 3H, Ar-CH<sub>3</sub>), 7.34 (d, 2H, *J* = 10 MHz, Ar-H), 7.71 (d, 2H, *J* = 10 MHz, Ar-H), 7.27 (s, 1H, Ar-H), 7.97 (s, 1H, -NH), 9.29 (s, 1H, -NH), 8.41 (m, 3H, Ar-H); <sup>13</sup>C NMR (500 MHz, DMSO-*d*<sub>6</sub>)  $\delta$  ppm: 160.81, 144.76, 142.28, 141.85, 129.94, 129.70, 129.06, 128.42, 128.02, 127.80, 127.45, 127.14, 126.22, 126.05, 125.01, 124.36, 122.05, 119.21, 118.09, 111.49, 110.51, 103.32, 40.59, 40.41, 40.24, 40.07, 39.91, 39.74, 39.57, 39.40, 26.17, 25.75, 21.45, 21.30; ESI-HRMS (*m/z*): 422.3129 [M-H]<sup>-</sup> (negative-ion mode).

**N-((2-Methyl-7-(trifluoromethyl)quinolin-4-yl)carbamoyl)-benzenesulfonamide (C2):** Yield: 53%; yellow crystalline; m.p.: 103 °C; m.f.: C<sub>18</sub>H<sub>14</sub>F<sub>3</sub>N<sub>3</sub>O<sub>3</sub>S; relative molecular mass: 422; FT-IR (ATR,  $\nu_{\max}$  cm<sup>-1</sup>): 3354.27 (2° amide N-H *str.*), 3257.83 (2° amide N-H *str.*), 1654.95 (C=O *str.*), 1525.72 (aromatic C=C *str.*); <sup>1</sup>H NMR (500 MHz, DMSO-*d*<sub>6</sub>)  $\delta$  ppm: 2.33 (s, 3H, Ar-CH<sub>3</sub>), 2.53 (s, 3H, Ar-CH<sub>3</sub>), 7.33 (d, 2H, *J* = 10 MHz, Ar-H), 7.70 (d, 2H, *J* = 5 MHz, Ar-H), 6.64 (s, 1H, Ar-H), 8.07 (s, 1H, -NH), 8.53 (s, 1H, -NH), 7.15 (d, 1H, *J* = 10 MHz, Ar-H), 7.57 (d, 1H, *J* = 10 MHz, Ar-H), 7.23 (s, 1H, Ar-H); <sup>13</sup>C NMR (500 MHz, DMSO-*d*<sub>6</sub>)  $\delta$  ppm: 161.01, 156.47, 156.22, 155.26, 142.28, 141.83, 141.33, 140.73, 129.70, 128.88, 128.85, 127.34, 127.28, 126.04, 125.79, 124.95, 124.34, 122.78, 120.84, 119.39, 118.17, 109.76, 103.54, 89.99, 40.40, 40.24, 40.07, 39.90, 39.73, 39.57, 39.40, 25.46, 21.37, 21.31, 21.28; ESI-HRMS (*m/z*): 422.3353 [M-H]<sup>-</sup> (negative-ion mode).

**N-((6-Fluoro-2-methylquinolin-4-yl)carbamoyl)-4-methylbenzenesulfonamide (C3):** Yield: 45%; yellow crystalline; m.p.: 174 °C; m.f.: C<sub>18</sub>H<sub>16</sub>FN<sub>3</sub>O<sub>3</sub>S; relative molecular mass: 373; FT-IR (ATR,  $\nu_{\max}$  cm<sup>-1</sup>): 3354.27 (2° amide N-H *str.*), 3257.83 (2° amide N-H *str.*), 1638.56 (C=O *str.*), 1559.47 (aromatic C=C



**Scheme-I:** Synthetic reaction scheme of sulfonylurea-linked quinoline derivatives (C1-C6)

*str.*;  $^1\text{H}$  NMR (500 MHz, DMSO- $d_6$ )  $\delta$  ppm: 2.34 (s, 3H, Ar-CH<sub>3</sub>), 2.53 (s, 3H, Ar-CH<sub>3</sub>), 7.70 (d, 2H,  $J$  = 10 MHz, Ar-H), 7.17 (d, 2H,  $J$  = 10 MHz, Ar-H), 6.58 (s, 1H, Ar-H), 7.26 (s, 1H, -NH), 8.60 (s, 1H, -NH), 7.57 (d, 1H,  $J$  = 5 MHz, Ar-H), 7.34 (d, 1H,  $J$  = 5 MHz, Ar-H), 7.23 (s, 1H, Ar-H);  $^{13}\text{C}$  NMR (500 MHz, DMSO- $d_6$ )  $\delta$  ppm: 160.42, 158.48, 157.39, 155.14, 153.68, 142.30, 141.83, 141.29, 136.39, 129.72, 128.86, 127.31, 126.04, 123.30, 123.11, 116.58, 116.51, 108.54, 108.34, 102.20, 40.41, 40.25, 40.08, 39.91, 39.75, 39.58, 39.41, 21.34, 21.32, 20.30; ESI-HRMS ( $m/z$ ): 372.3357 [M-H]<sup>-</sup> (negative-ion mode).

***N*-((7-Fluoroquinolin-4-yl)carbamoyl)-4-methylbenzenesulfonamide (C4):** Yield: 58%; white crystalline; m.p.: 160 °C; m.f.: C<sub>17</sub>H<sub>14</sub>FN<sub>3</sub>O<sub>3</sub>S; relative molecular mass: 359; FT-IR (ATR,  $\nu_{\text{max}}$  cm<sup>-1</sup>): 3351.37 (2° amide N-H *str.*), 3257.83 (2° amide N-H *str.*), 1599.02 (C=O *str.*), 1477.50 (aromatic C=C *str.*);  $^1\text{H}$  NMR (500 MHz, DMSO- $d_6$ )  $\delta$  ppm: 2.33 (s, 3H, Ar-CH<sub>3</sub>), 7.71 (d, 2H,  $J$  = 10 MHz, Ar-H), 7.34 (d, 2H,  $J$  = 10 MHz, Ar-H), 7.28 (s, 1H, -NH), 8.88 (s, 1H, -NH), 8.58 (d, 1H,  $J$  = 5 MHz, Ar-H), 8.14 (d, 1H,  $J$  = 5 MHz, Ar-H), 7.78 (d, 1H,  $J$  = 10 MHz, Ar-H), 7.59 (d, 1H,  $J$  = 10 MHz, Ar-H), 6.74 (d, 1H,  $J$  = 5 MHz, Ar-H);  $^{13}\text{C}$  NMR (500 MHz, DMSO- $d_6$ )  $\delta$  ppm: 163.73, 159.25, 158.16, 151.23, 144.95, 143.43, 142.30, 141.83, 135.20, 129.72, 128.98, 128.91, 127.54, 127.40, 127.26, 126.05, 125.55, 116.95, 116.57, 116.24, 116.03, 114.66,

113.71, 107.66, 105.26, 102.52, 79.09, 40.40, 40.23, 40.06, 39.90, 39.73, 39.56, 39.39, 38.67, 21.33, 17.35; ESI-HRMS ( $m/z$ ): 358.3165 [M-H]<sup>-</sup> (negative-ion mode).

***N*-((2,8-Bis(trifluoromethyl)quinolin-4-yl)carbamoyl)-4-methylbenzenesulfonamide (C5):** Yield: 64%; white crystalline; m.p.: 132 °C; m.f.: C<sub>19</sub>H<sub>13</sub>F<sub>6</sub>N<sub>3</sub>O<sub>3</sub>S; relative molecular mass: 477; FT-IR (ATR,  $\nu_{\text{max}}$  cm<sup>-1</sup>): 3288.63 (2° amide N-H *str.*), 3258.79 (2° amide N-H *str.*), 1700.28 (C=O *str.*), 1596.12 (aromatic C=C *str.*);  $^1\text{H}$  NMR (500 MHz, DMSO- $d_6$ )  $\delta$  ppm: 2.34 (s, 3H, Ar-CH<sub>3</sub>), 7.71 (d, 2H,  $J$  = 10 MHz, Ar-H), 7.34 (d, 2H,  $J$  = 10 MHz, Ar-H), 7.27 (s, 1H, -NH), 9.70 (s, 1H, -NH), 7.92 (d, 1H,  $J$  = 5 MHz, Ar-H), 7.44 (d, 1H,  $J$  = 5 MHz, Ar-H), 8.40 (d, 1H,  $J$  = 10 MHz, Ar-H), 8.29 (d, 1H,  $J$  = 10 MHz, Ar-H), 8.46 (s, 1H, Ar-H);  $^{13}\text{C}$  NMR (500 MHz, DMSO- $d_6$ )  $\delta$  ppm: 149.74, 148.06, 147.79, 144.99, 144.91, 143.86, 142.28, 141.85, 136.58, 130.35, 130.14, 129.70, 128.16, 127.67, 126.56, 126.05, 125.11, 120.78, 104.96, 40.40, 40.23, 40.06, 39.90, 39.73, 39.56, 39.39, 21.48, 21.30; ESI-HRMS ( $m/z$ ): 476.3896 [M-H]<sup>-</sup> (negative-ion mode).

***N*-((7-(1,1-Difluoroethyl)quinolin-4-yl)carbamoyl)-4-methylbenzenesulfonamide (C6):** Yield: 17%; white crystalline; m.p.: 118 °C; m.f.: C<sub>19</sub>H<sub>17</sub>F<sub>2</sub>N<sub>3</sub>O<sub>3</sub>S; relative molecular mass: 409; FT-IR (ATR,  $\nu_{\text{max}}$  cm<sup>-1</sup>): 3349.45 (2° amide N-H *str.*), 3257.83 (2° amide N-H *str.*), 1653.02 (C=O *str.*), 1598.05



(aromatic C=C *str.*);  $^1\text{H}$  NMR (500 MHz,  $\text{DMSO}-d_6$ )  $\delta$  ppm: 2.34 (s, 3H, Ar- $\text{CH}_3$ ), 7.71 (d, 2H,  $J = 10$  MHz, Ar-H), 7.34 (d, 2H,  $J = 10$  MHz, Ar-H), 7.27 (s, 1H, -NH), 8.46 (s, 1H, -NH), 6.80 (d, 1H,  $J = 5$  MHz, Ar-H), 8.55 (d, 1H,  $J = 10$  MHz, Ar-H), 8.13 (s, 1H, Ar-H), 7.59 (d, 1H,  $J = 10$  MHz, Ar-H), 7.16 (d, 1H,  $J = 5$  MHz, Ar-H);  $^{13}\text{C}$  NMR (500 MHz,  $\text{DMSO}-d_6$ )  $\delta$  ppm: 156.29, 155.22, 152.55, 146.61, 142.30, 141.84, 141.35, 129.71, 128.94, 128.88, 127.39, 127.29, 126.05, 125.86, 124.58, 120.98, 119.40, 109.77, 103.83, 40.40, 40.23, 40.07, 39.90, 39.73, 39.57, 39.40, 21.32, 21.30; ESI-HRMS ( $m/z$ ): 408.3487  $[\text{M}-\text{H}]^-$  (negative-ion mode).

***P. falciparum* parasite:** The parasite culture method was similar to those described earlier [8]. The *P. falciparum* lab strain 3D7 (provided by University Malaya) was grown in washed human O<sup>+</sup> red blood cells and maintained in culture with the prepared malaria complete medium (MCM). The parasites were incubated in sealed flasks and maintained *in vitro* at 37 °C and were subjected to microaerophilic conditions (5% O<sub>2</sub>, 5% CO<sub>2</sub> and 90% N<sub>2</sub>), supplied in the form of a dedicated gas cylinder (Linde, Germany). Every two days, the medium was changed and the level of parasitaemia was checked. Blood smears were prepared, fixed in methanol and air-dried. The slides were stained with 20% Giemsa for 45 min and observed at 100x magnification under oil immersion. Approximately, 1000 red blood cells per smear were counted and the parasitaemia (%) was calculated as:

$$\text{Parasitaemia (\%)} = \frac{\text{Number of parasitized RBCs (iRBCs)}}{\text{Total number of RBCs}} \times 100$$

**Preparation of test concentration:** A 100 mM stock solution of the test compounds **C1-C6** were prepared by dissolving the compounds in 100% DMSO. The prepared stock solutions were further diluted in MCM to the desired concentration of 100  $\mu\text{M}$ . A 50  $\mu\text{L}$  of test compounds were pre-dosed in the 96-well flat-bottom black cell culture plate (SPL Life Sciences, Korea) and kept at 4 °C, which were used within 1 day after preparation.

**Malaria SYBR green assay:** Asynchronous parasites were used, with starting parasitaemia no less than 2.5%. A 50  $\mu\text{L}$  of parasitized red blood cells (1% parasitaemia and 5% haematocrit) was added to each well of the pre-dosed 96-well flat bottom black cell culture plate containing test compounds in triplicates at desirable concentrations. DMSO alone without parasitized red blood cells, non-parasitized red blood cells, parasitized red blood cells and artesunate were used as fluorescence control, reference control, negative control and positive control, respectively. The final concentration of DMSO in the assay was at 0.1%. Following this, the plate was placed in an airtight Tupperware, gassed with 5% O<sub>2</sub>, 5% CO<sub>2</sub> and 90% N<sub>2</sub> and incubated at 37 °C for 72 h. The assay was terminated by freezing the plate at -80 °C overnight. After thawing for 2 h, each well was added with 50  $\mu\text{L}$  SYBR Green I lysis buffer containing 20 mM Tris(hydroxymethyl)aminomethane (TRIS) (1<sup>st</sup> Base, Singapore), 5 mM ethylenediaminetetraacetic acid (EDTA) (R&M Chemicals, U.K.), 0.008% (w/v) saponin (Sigma-Aldrich, Germany), 0.08% (v/v) Triton<sup>TM</sup> X-100 (Sigma-Aldrich) and 1X SYBR Green nucleic acid dye (Invitrogen by

Thermo-Fisher Scientific). The plates were placed on the Stovall Belly Dancer shaker for 30 min at room temperature for thorough mixing. This was followed by measurement of the fluorescence intensities at excitation/emission wavelength = 485/528 nm using the Tecan Infinite 200 Pro M Plex microplate reader. The parasite growth percentages were determined using the formula:

$$\text{Parasite growth (\%)} = \frac{\text{FL}_{\text{sample}} - \text{FL}_{\text{uRBC}}}{\text{FL}_{\text{iRBC}}} \times 100$$

where  $\text{FL}_{\text{sample}}$  is the fluorescence intensity of treated parasites,  $\text{FL}_{\text{uRBC}}$  is the fluorescence intensity of sample background and  $\text{FL}_{\text{iRBC}}$  is the fluorescence intensity of untreated parasitized RBCs.

**Statistical analysis:** The descriptive statistics was analyzed using Microsoft Excel software.

## RESULTS AND DISCUSSION

The physical and spectral properties of synthesized sulfonyl-urea-linked quinoline derivatives (**C1-C6**) presented above were interpreted to elucidate the molecular structure of the compounds. The relative molecular mass of the synthesized compounds was confirmed based on the pseudo-molecular ion  $[\text{M}-\text{H}]^-$  that was observed in their high-resolution mass spectroscopy (HRMS) in negative-ion mode, which is, the mass-to-charge ratio ( $m/z$ ) signal at 422.3129 for **C1**, 422.3353 for **C2**, 372.3357 for **C3**, 358.3165 for **C4**, 476.3896 for **C5** and 408.3487 for **C6**. The vibrational spectrum (FT-IR in ATR mode) of molecule **C1** showed prominent bands at 3349.45 and 3258.79  $\text{cm}^{-1}$ , indicating N-H stretching frequencies of 2° amido group, at 1688.71  $\text{cm}^{-1}$  for C=O stretching of a carbonyl group and at 1576.83  $\text{cm}^{-1}$  for C=C aromatic stretching. The  $^1\text{H}$  NMR (500 MHz,  $\text{DMSO}-d_6$ ) revealed peaks for aromatic methyl group protons at  $\delta$  2.35 ppm and  $\delta$  2.56 ppm (singlets, three protons each), aromatic ring protons at  $\delta$  7.34 ppm and  $\delta$  7.71 ppm (doublets, two protons each,  $J = 10$  Hz) and amino protons at  $\delta$  7.97 ppm and  $\delta$  9.29 ppm (singlets, one proton each), with the total aromatic protons matching the theoretical value. The  $^{13}\text{C}$  NMR spectrum displayed characteristic peaks at  $\delta$  160.81 ppm for carbonyl carbon and  $\delta$  21.30 ppm for aromatic methyl carbon, with all observed carbon signals consistent with the theoretical backbone of molecule **C1**. For molecule **C2**, the vibrational spectrum displayed characteristic bands at 3354.27  $\text{cm}^{-1}$  and 3257.83  $\text{cm}^{-1}$  for N-H stretching of 2° amido group, 1654.95  $\text{cm}^{-1}$  for C=O stretching of carbonyl group and 1525.72  $\text{cm}^{-1}$  for C=C aromatic stretching of the aromatic bond. The  $^1\text{H}$  NMR (500 MHz) spectrum in  $\text{DMSO}-d_6$  showed singlets at  $\delta$  2.33 ppm and  $\delta$  2.53 ppm (three-proton integrations each) for aromatic methyl group protons, doublets at  $\delta$  7.33 ppm ( $J = 10$  MHz) and  $\delta$  7.70 ppm ( $J = 5$  MHz) for aromatic ring protons and singlets at  $\delta$  8.07 ppm and  $\delta$  8.53 ppm (one-proton integrations each) for amino protons. The remaining aromatic protons matched the theoretical proton count. The  $^{13}\text{C}$  NMR spectrum exhibited a peak at  $\delta$  161.01 ppm for carbonyl carbon,  $\delta$  21.28 ppm for the aromatic methyl carbon and other peaks consistent with aromatic carbons, aligning with the theoretical structure of molecule **C2**. In case of molecule **C3**, the FT-IR spectrum

showed characteristic bands at  $3354.27\text{ cm}^{-1}$  and  $3257.83\text{ cm}^{-1}$  for N-H stretching frequencies of the  $2^\circ$  amido group, at  $1638.56\text{ cm}^{-1}$  for C=O stretching of the carbonyl group and at  $1559.47\text{ cm}^{-1}$  for C=C aromatic stretching. The  $^1\text{H}$  NMR (500 MHz) spectrum revealed singlet peaks at  $\delta$  2.34 ppm and  $\delta$  2.53 ppm for three aromatic methyl group protons, doublet peaks at  $\delta$  7.70 ppm and  $\delta$  7.17 ppm for two aromatic ring protons ( $J = 10\text{ Hz}$ ) and singlet peaks at  $\delta$  7.26 ppm and  $\delta$  8.60 ppm for one amino proton each. The aromatic proton integrations were consistent with the theoretical values.

The  $^{13}\text{C}$  NMR spectrum of **C3** showed peaks at  $\delta$  160.42 ppm for the carbonyl carbon and at  $\delta$  21.32 ppm for the aromatic methyl carbon, with other peaks matching the expected aromatic carbons, confirming the theoretical structure of **C3**. Likewise compound **C4**, the FT-IR (ATR mode) spectrum revealed key vibrational frequencies: bands at  $3351.37\text{ cm}^{-1}$  and  $3257.83\text{ cm}^{-1}$  indicating N-H stretching of  $2^\circ$  amido group; a band at  $1599.02\text{ cm}^{-1}$  for C=O stretching of the carbonyl group; and a band at  $1477.50\text{ cm}^{-1}$  corresponding to C=C aromatic stretching. The  $^1\text{H}$  NMR (500 MHz) spectrum in  $\text{DMSO}-d_6$  showed various proton signals, including a singlet at  $\delta$  2.33 ppm (aromatic methyl group, 3 protons), doublets at  $\delta$  7.71 ppm and  $\delta$  7.34 ppm (aromatic ring protons, 2 protons each,  $J = 10\text{ MHz}$ ), singlets at  $\delta$  7.28 ppm and  $\delta$  8.88 ppm (amino protons, 1 proton each), with a total of five aromatic ring protons matching theoretical expectations. In the same order, the FT-IR spectrum of molecule **C5** in ATR mode shows significant bands at  $3288.63\text{ cm}^{-1}$  and  $3258.79\text{ cm}^{-1}$ , indicating N-H stretching of  $2^\circ$  amido group. A band at  $1700.28\text{ cm}^{-1}$  suggests C=O stretching of the carbonyl group, while a band at  $1596.12\text{ cm}^{-1}$  corresponds to C=C aromatic stretching of the aromatic C=C bond. The  $^1\text{H}$  NMR spectrum of molecule **C5** in  $\text{DMSO}-d_6$  reveals various proton signals: a singlet at  $\delta$  2.34 ppm (three-proton integration) for aromatic methyl protons, doublets at  $\delta$  7.71 ppm and  $\delta$  7.34 ppm (two-proton integration each,  $J = 10\text{ MHz}$ ) for aromatic ring protons, a singlet at  $\delta$  7.27 ppm (one-proton integration) for an amino proton and a singlet at  $\delta$  9.70 ppm (one-proton integration) for another amino proton. The aromatic protons integrate in agreement with the theoretical values. The  $^{13}\text{C}$  NMR spectrum of **C5** shows a peak at  $\delta$  149.74 ppm for the carbonyl carbon and a peak at  $\delta$  21.30 ppm for the aromatic methyl carbon. Additional carbon peaks confirm the presence of aromatic carbons, matching the theoretical structure of the compound. Lastly, the FT-IR spectrum of molecule **C6** in ATR mode showed key vibrational frequencies: a broad band at  $3349.45\text{ cm}^{-1}$  and  $3257.83\text{ cm}^{-1}$ , indicating the presence of two N-H stretching frequencies of the secondary amido group, a prominent band at  $1653.02\text{ cm}^{-1}$  for C=O stretching of the carbonyl group and a band at  $1598.05\text{ cm}^{-1}$  for C=C aromatic stretching. The  $^1\text{H}$  NMR revealed proton types with specific chemical shifts: a singlet at  $\delta$  2.34 ppm for the aromatic methyl group, doublets at  $\delta$  7.71 ppm and  $\delta$  7.34 ppm ( $J = 10\text{ MHz}$ ) for aromatic ring protons, singlets at  $\delta$  7.27 ppm and  $\delta$  8.46 ppm for amino protons and integration of five other aromatic protons matching the theoretical count. The  $^{13}\text{C}$  NMR (500 MHz) showed characteristic peaks at  $\delta$  156.29 ppm for the carbonyl carbon,  $\delta$  21.30 ppm for the aromatic methyl carbon and other

peaks corresponding to aromatic carbons, closely aligning with the theoretical structure of the compound.

#### Antimalarial activity screening against *P. falciparum*:

As part of evaluating antimalarial potential, we systematically assessed the biological activity of six synthesized compounds **C1-C6** alongside a known reference compound, artesunate, by measuring the % inhibition of iRBC for each compound. This approach allowed us to establish a clear structure-activity relationship (SAR) by observing varying effects of the substituents on the quinoline structure and identifying how these modifications influenced effectiveness. The compounds are found in their decreasing order of potency: **C3** (68.10%) > **C2** (65.55%) > artesunate (64.98%) > **C4** (63.99%) > **C6** (40.39%) > **C1** (38.23%) > **C5** (inactive) (Table-1). The trend shows that **C3** is the most potent hit molecule; in addition, **C2** is ranked second best, with more promising activity than the standard artesunate (64.8%). Compound **C4** is relatively less than the standard but close to the standard, whereas compounds **C6** and **C1** were reported as low activity and **C5** is a fully inactive compound, as shown in Figs. 1 and 2.

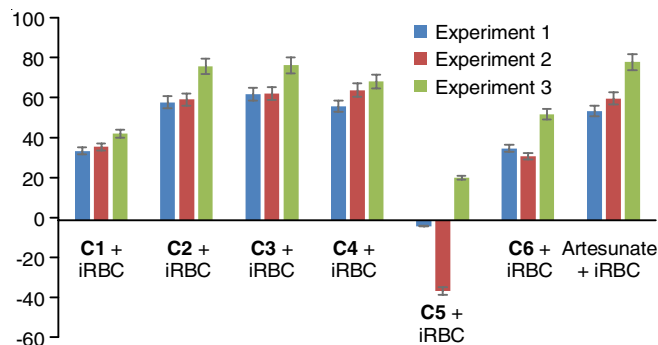


Fig. 1. Percentage inhibition of infected red-blood cells (iRBC) by sulfonylurea-linked quinolines (**C1-C6**) in triplicate experiments

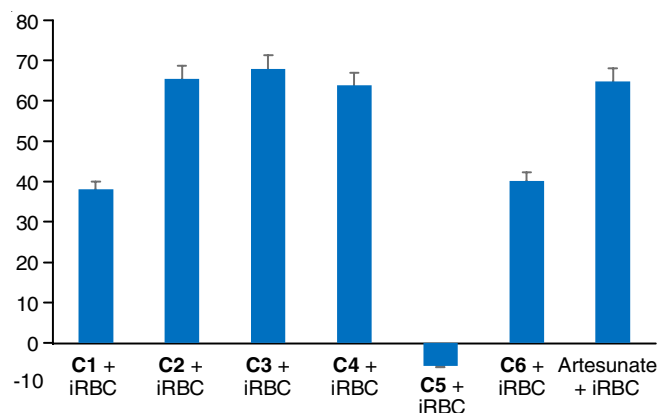
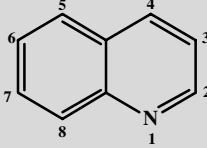


Fig. 2. Average percentage inhibition of infected red-blood cells (iRBC) by sulfonylurea-linked quinolines (**C1-C6**)

**SAR studies:** A deeper insight into the structure-activity relationships (SAR) for the quinoline derivatives (**C1-C6**) screened for their antimalarial properties. The role of chemical features in various aspects was elucidated, such as the role of substituent functional groups at different positions on the quinoline ring system, relative comparisons among electron-donating and electron-withdrawing groups and further possi-

TABLE-1  
AVERAGE PERCENTAGE INHIBITION OF THE *Plasmodium falciparum* INFECTED RED BLOOD CELL (iRBC) OF COMPOUNDS **C1-C6**

Compound	Average % Inhibition of infected red blood cell (iRBC)	Name of the substituent on the quinoline/chemical nature of the substituent			
					
		Quinoline position 1	Quinoline position 2	Quinoline position 3	Quinoline position 4
<b>C1</b>	38.23	No substituent	Methyl/electron-donating	No substituent	Tosylurea/electron-withdrawing
<b>C2</b>	65.55	No substituent	Methyl/electron-donating	No substituent	Tosylurea/electron-withdrawing
<b>C3</b>	68.10	No substituent	Methyl/electron-donating	No substituent	Tosylurea/electron-withdrawing
<b>C4</b>	63.99	No substituent	No substituent	No substituent	Tosylurea/electron-withdrawing
<b>C5</b>	Inactive	No substituent	Trifluoromethyl/ electron-withdrawing	No substituent	Tosylurea/electron-withdrawing
<b>C6</b>	40.39	No substituent	No substituent	No substituent	Tosylurea/electron-withdrawing
		Quinoline position 5	Quinoline position 6	Quinoline position 7	Quinoline position 8
		<b>C1</b>	38.23	No substituent	Trifluoromethyl/electron-withdrawing
		<b>C2</b>	65.55	No substituent	No substituent
		<b>C3</b>	68.10	No substituent	No substituent
		<b>C4</b>	63.99	No substituent	No substituent
		<b>C5</b>	Inactive	No substituent	Trifluoromethyl/electron-withdrawing
		<b>C6</b>	40.39	No substituent	Trifluoromethyl/electron-withdrawing
Artesunate	64.98				

bilities for the optimization. The systematic SAR analysis investigates the antimalarial properties of quinoline derivatives **C1-C6**, highlighting their inhibitory activity against infected red blood cells (iRBCs). The observed % inhibition of iRBC values of compounds **C1-C6** revealed the significant role of substituent positioning on the quinoline and their electronic properties in determining antimalarial potency. The activity data for quinoline derivatives **C1-C6** and artesunate showed a range of % inhibition values against iRBCs: **C1**: 38.23%, **C2**: 65.55%, **C3**: 68.10% (highest activity), **C4**: 63.99%, **C5**: inactive, **C6**: 40.39%, artesunate: 64.98% (positive standard). The SAR of quinoline derivatives was studied based on various substituents at positions 2, 4, 6 and 8, while other positions 1, 3, 5 and 7 were unsubstituted. A relationship when analyzing the role of these substituents at positions 2, 4, 6 and 8 in modulating % inhibition is observed. However, we discussed the effect of substituents at all positions on the quinoline ring: As in the case of position 1 on the quinoline scaffold, it remains unsubstituted across all compounds. This observation suggests that the lack of a substituent at position 1 does not contribute to the activity either positively or negatively. From a structural perspective, this site may not directly interact with the biological target or steric hindrance at this position could reduce binding affinity. Secondly, position 2 showed the presence of a methyl group in compounds **C1** to **C4**, contributing positively to activity. The methyl group acts as an electron-donating substituent that increases the electron density on the quinoline ring. This structural enhancement may exhibit favourable molecular

interactions with the hydrophobic binding pockets in the parasite target site. Influence of position 2 substitution: **C1**: methyl group, 38.23%; **C2**: methyl group, 65.55%; **C3**: methyl group, 68.10% (peak activity). **C4**: absence of position 2 substitution indicates the correlation with decreased activity (63.99%); **C5**: absence of substitution at position 2 and inactivity (0%). These observations revealed that the methyl group at position 2 is essential for the activity. However, the slight decrease in activity from **C3** to **C4** indicates other positions also play a critical role in modulating efficacy. On the other side, none of the compounds has substitution at position 3. From this observation, it appears that the substitution at position 3 is not essential for standard activity; it represents an unexplored position for the optimization. Introducing polar or hydrogen-bonding groups here could enhance target interactions or improve solubility. In addition, the tosylurea group is consistently present at position 4 in all active compounds (**C1-C4** and **C6**). This group is electron withdrawing, suggesting it might facilitate ligand interactions with electron-deficient sites on the biological target. Moreover, its bulky structure might contribute steric stabilization, enhancing binding specificity. It is noteworthy to take note that the inactive compound **C5** still retains the tosylurea group but lacks other important substituents, such as methyl group at position 2 and the fluoro group at position 6. This implies that substitution with tosylurea alone does not guarantee the activity. Position 5 is consistently unsubstituted across all compounds. Similar to position 1, this site may lack direct involvement in target interactions. Introducing substituents here might alter the elect-



ronic environment or binding dynamics. The presence of fluoro and trifluoromethyl groups at position 6 in compounds **C3** and **C4** correlates with high activity: **C3** (68.10%): fluoro group at position 6, **C4** (63.99%): fluoro group at position 6, **C5** (inactive): absence of substitution at position 6, fluoro and trifluoromethyl groups are strong electron-withdrawing substituents, enhancing target binding by stabilizing electronic interactions. The high activity of **C3** highlights the importance of fluoro group in this position. No substituents are present at position 7, suggesting it does not play a direct role in biological activity. Like positions 3 and 5, this site remains a potential candidate for modification in future SAR studies. Position 8 features a trifluoromethyl group in several compounds (e.g. **C1** and **C6**), contributing to moderate activity levels: **C1** (38.23 %): trifluoromethyl group at position 8; **C6** (40.39%): trifluoromethyl group at position 8. The electron-withdrawing nature of the trifluoromethyl group likely enhances binding affinity by interacting with electron-deficient regions on the target. However, its absence in more active compounds, such as **C3**, suggests its effects are not equivalently positive. Artesunate, a structurally distinct clinically used first-line antimalarial agent that exhibits 64.98% inhibition of iRBCs. Its comparable activity highlights the versatility of diverse scaffolds in achieving similar biological effects. The performance of artesunate provides a benchmark for evaluating the potency of quinoline derivatives **C1-C6**, underlining the need for a combination of electronic and steric properties to optimize efficacy. Some mechanistic insights, such as electron-donating groups enhancing activity at position 2: methyl substitution at position 2 consistently enhances % inhibition, likely due to increased hydrophobic interactions and electron density. Tosylurea substitution produces essential baseline activity: the presence of tosylurea across all active compounds indicates its role as a key pharmacophore. Electron-withdrawing groups at position 6 are critical for peak activity: fluoro and trifluoromethyl groups at position 6 significantly enhance activity, as evidenced by compounds **C3** and **C4**. Inactive compound **C5** underscores the necessity of synergistic interactions between substituents at positions 2, 4 and 6. Strategies to optimize drug-like properties of a bioactive ligand by exploring the influence of substitution at positions 1, 3, 5 and 7, which were not explored in this study. Synthesis of new molecules by introducing polar or hydrogen-bonding groups at these positions could optimize pharmacokinetics and binding interactions. Likewise, the use of computational studies to design virtual ligands and identify their binding properties, like binding energy, binding orientation and binding interactions, could predict the ability to be antimalarial agents; in addition, bioisosteres replacement of methyl, trifluoromethyl or fluoro groups with other groups would be remarkable for the ligand optimization. Combining electron-donating and electron withdrawing groups in novel patterns may yield synergistic effects against multi-drug-resistant malaria strains. The SAR analysis of quinoline derivatives **C1-C6** provided valuable insights into the structural features influencing *in vitro* antimalarial activity. By leveraging the findings from this study, we can further focus on optimizing the quinoline scaffold for enhanced efficacy, paving the way for novel therapeutics to treat malaria.

## Conclusion

The ongoing challenge of malaria remains a significant global health issue, as highlighted by the WHO's alarming statistics on rising mortality rates, emphasizing the urgent need for new treatments. In this study, a series of sulfonylurea-linked quinoline derivatives **C1-C6**, synthesized, characterized and evaluated their effectiveness against *P. falciparum*, revealing that compounds **C3** and **C2** emerged as the most promising candidates, achieving remarkable inhibition rates of 68.10% and 65.55%, respectively, comparable to the established antimalarial drug artesunate. The success of these compounds can be attributed to their hybrid pharmacophoric features, tosylurea and quinoline, which are forming part of the basic nucleus. The established SARs in this study guide the design of more effective analogues in future studies.

## ACKNOWLEDGEMENTS

All the authors are thankful to the IMU University Vice Chancellor, Dean, School of Pharmacy; Dean, School of Postgraduate Studies; Director and Deputy Directors of the Institute for Research, Development & Innovation (IRDI) for providing the facilities to complete the proposed research project. This research project was funded by IMU University Joint-Committee on Research & Ethics, Project IDs No. MSc in Molecular Medicine: MMM I/2021(01).

## CONFLICT OF INTEREST

The authors declare that there is no conflict of interests regarding the publication of this article.

## REFERENCES

1. P. Venkatesan, *Lancet Microbe*, **5**, e214 (2024); [https://doi.org/10.1016/S2666-5247\(24\)00016-8](https://doi.org/10.1016/S2666-5247(24)00016-8)
2. M. Fikadu and E. Ashenafi, *Infect. Drug Resist.*, **16**, 3339 (2023); <https://doi.org/10.2147/IDR.S405668>
3. F.O. Maiga, M. Wele, S.M. Toure, M. Keita, C.O. Tangara, R.R. Refeld, O. Thiero, K. Kayentao, M. Diakite, A. Dara, J. Li, M. Toure, I. Sagara, A. Djimdé, F.J. Mather, S.O. Doumbia and J.G. Shaffer, *Malaria J.*, **20**, 356 (2021); <https://doi.org/10.1186/s12936-021-03890-0>
4. H. Tripathi, P. Bhalariao, S. Singh, H. Arya, B.S. Alotaibi, S. Rashid, M.R. Hasan and T.K. Bhatt, *Parasites Vectors*, **16**, 130 (2023); <https://doi.org/10.1186/s13071-023-05755-8>
5. H. Behzadi and K.K. Zborowski, *Targets*, **3**, 1 (2025); <https://doi.org/10.3390/targets3010001>
6. C. León, J. Rodrigues, N. Gamboa de Domínguez, J. Charris, J. Gut, P.J. Rosenthal and J.N. Domínguez, *Eur. J. Med. Chem.*, **42**, 735 (2007); <https://doi.org/10.1016/j.ejmech.2007.01.001>
7. F.-F. Meng, M.-H. Shang, W. Wei, Z.-W. Yu, J.-L. Liu, Z.-M. Li, Z.-W. Wang, J.-G. Wang and H.-Q. Dai, *Antibiotics*, **12**, 323 (2023); <https://doi.org/10.3390/antibiotics12020323>
8. F.S.F. Yasmin, S.K. Priadarsshini, S.K. Sharanya, W.Y. Wan, K.L. Tim and A.V. Rao, *Res. J. Biotechnol.*, **20**, 50 (2025); <https://doi.org/10.25303/201rjbt050054>
9. T.T. Bui, D.Q. Ngo and V.L. Tran, *Vietnam J. Sci. Technol. Eng.*, **62**, 32 (2020); [https://doi.org/10.31276/VJSTE.62\(2\).34-37](https://doi.org/10.31276/VJSTE.62(2).34-37)
10. N. Li, Y. Wang, W. Li, H. Li, L. Yang, J. Wang, H.A. Mahdy, A.B.M. Mehany, D.A. Jaiash, E.Y. Santali and I.H. Eissa, *J. Chem.*, **2020**, 1631243 (2020); <https://doi.org/10.1155/2020/1631243>
11. A.N. Suresh, A.S.A. Luang, M.C.Y. Ling, T.N. Selvam and V.R. Avupati, *Asian J. Chem.*, **36**, 2467 (2024); <https://doi.org/10.14233/ajchem.2024.32383>